A Snapshot of Turbulence in the Northeastern Strait of Magellan

I. D. Lozovatsky[1], C. Escauriaza[3], L. Suarez[3,4], H. J. S. Fernando[1,2], M. E. Williams[5], R. S. Coppersmith[1], and N. Mayorga[3]

[1]Department of Civil & Environmental Engineering & Earth Sciences, University of Notre Dame, USA

[2]Department of Aerospace and Mechanical Engineering, University of Notre Dame, USA

[3]Departmento de Ingeniería Hidráulica y Ambiental. Pontificia Universidad Católica de Chile, Chile

[4]Marine Energy Research & Innovation Center (MERIC), Santiago, Chile.

[5]Departmento de Obras Civiles. Universidad Técnica Federico Santa María, Valparaíso, Chile

Corresponding author Iossif Lozovatsky (i.lozovatsky@nd.edu)

Key Points:

- Results of first ever direct measurements of small-scale turbulence in the Strait of Magellan conducted using a microstructure profiler VMP-500 are reported.
- Above the bottom boundary layer, the probability distribution of turbulent kinetic energy (TKE) dissipation rate was lognormal with a median exceeding 10^{-6} Wkg^{-1}.
- In the BBL, the mean shear and TKE dissipation rate decreased exponentially with the distance from the seafloor ζ leading to an eddy viscosity ~ 10^{-3} m^2s^{-1} independent on ζ.

Abstract

First-ever measurements of the turbulent kinetic energy (TKE) dissipation rate in the northeastern Strait of Magellan (Segunda Angostura region) taken in March 2019 are reported here. At the time of microstructure measurements, the magnitude of the reversing tidal current ranged between 0.8 and 1.2 ms^{-1}. The probability distribution of the TKE dissipation rate in the water interior above the bottom boundary layer was lognormal with a high median value $\varepsilon_{med}^{MS} = 1.2 \times 10^{-6}$ Wkg^{-1}. Strong vertical shear, $(1-2) \times 10^{-2}$ s^{-1} in the weakly stratified water interior ensued a sub-critical gradient Richardson number, $Ri < 10^{-1} - 10^{-2}$. In the bottom boundary layer (BBL), the vertical shear and the TKE dissipation rate both decreased exponentially with the distance from the seafloor ζ, leading to a turbulent regime with the eddy viscosity $K_M \sim 10^{-3}$ m^2/s, which varied with the time and location, while being independent of the vertical coordinate in the upper part of BBL (for $\zeta > \sim 2$ meters above the bottom).

Plain Language Summary

The Strait of Magellan (MS) is a narrow ~ 2 km wide and ~ 500 km long waterway that meanders between the Atlantic and Pacific oceans, separating Patagonia from Tierra del Fuego. The Strait is an environmentally unique, and undergoes rapid ecological changes due to anthropogenic stressors. To study small-scale marine turbulence in the region, which influences vertical transport of heat, momentum, nutrients, sediments and other substances, we conducted first ever direct measurements of turbulent kinetic energy (TKE) dissipation rate ε in the northeastern part of the Strait (Segunda Angostura narrow) using a vertical microstructure profiler. The most notable finding is the very high level of turbulence existing near the seafloor, signified by $\varepsilon_b \approx 10^{-3}$ Wkg^{-1}, which is among the highest TKE dissipation rate measured previously by numerous authors in various narrow tidal channels. Tidal currents in MS generated a turbulent bottom boundary layer (BBL) with an exponential decay of the dissipation rate and the mean velocity gradient (vertical shear) toward the water interior. This turbulent regime can be specified by the eddy viscosity on the order of $\sim 10^{-3}$ m^2/s that varied with time and location while being independent of the vertical coordinate ζ in the upper part of BBL (for $\zeta > \sim 2$ meters above the bottom). The measurements described has only limited information on the specifics of turbulence in MS, calling for further investigations of turbulence and mixing therein.

1 Introduction

The Strait of Magellan (henceforth also the Magellan Strait (MS) or just the Strait) is an environmentally unique region being, in particular, a feeding ground to humpback whales (Acevedo et al., 2011). The region currently experiences changes of its ecological balance due to anthropogenic stressors such as excessive fishing, offshore oil production and newly leased areas for aquaculture. Understanding of small-scale dynamical processes in the Magellan Strait is paramount for multidisciplinary studies of physical, biogeochemical and ecological processes in the coastal regions of Patagonia. For this reason, we launched the first ever in-situ measurements of the kinetic energy dissipation rate in the north-eastern part of the Strait to obtain estimates of turbulence and mixing across the water column down to the bottom boundary layer (BBL).

The Strait of Magellan is a narrow ~ 1.1 nautical miles (NM) waterway that meanders between the Atlantic and Pacific oceans, separating Patagonia from Tierra del Fuego; it is about 310 NM long (Figure 1). According to Simeoni et al. (1997), the mean annual air temperature of the eastern MS is 6 - 7° C, varying from 8° to 11°C in the summer (December - February) and from 2° to 3° C in the winter (June-August). Easterly-directed winds of characteristic speed 7 ms^{-1} are typical in the region (Garreaud et al., 2013). Stormy winds (up to 25 ms^{-1}) are often observed during winter and spring seasons.

Strong barotropic tidal flow and winds are the major drivers of mesoscale circulation in the Strait. On the Atlantic side, the Strait is characterized by high-amplitude semidiurnal tides with a mean tide range of 7.1 m, which gradually decreases to about 1.5 - 2 m toward Punta Arenas (see Figure 4 of Medeiros & Kjerfve, 1988). Tidal amplification occurs in a series of narrows at the Atlantic side to the northeast of Punta Arenas (Figure 1), for example, in Segunda Angostura (SA), where our pilot field campaign was conducted (see also detailed map of SA in Figure 1 of Lutz et al., 2016). The seabed in SA is mainly composed of hard substratum and outcropping rocks (Simeoni et al., 1997). High level of tidally induced turbulence is an expected phenomenon in SA as has been reported in several recent publications on turbulence in narrow tidal channels elsewhere (e.g., McMillan et al., 2016; Horwitz & Hay, 2017; Guerra & Thomson, 2017; Ross et al., 2019).

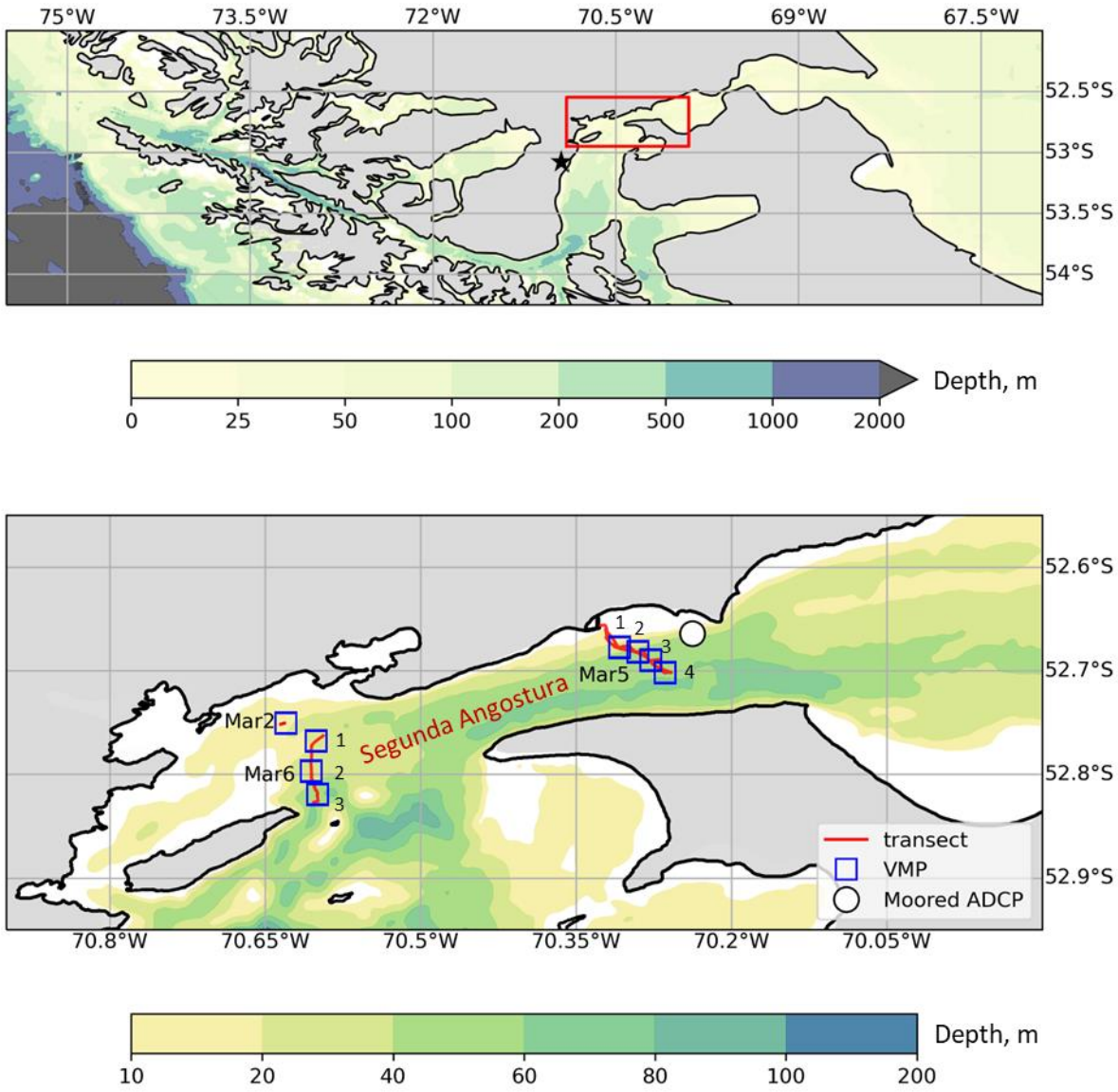

Figure 1. Upper panel: the measurement site (bounded by a red box) in the main passage of the Magellan Strait to the NNE from Punta Arenas (black star). Lower panel: an enlarged section of the Magellan Strait showing locations of the VMP stations (squares marked by the date and station numbers); the ADCP mooring (a white circle). Two separate color palettes (scales) specify the mean water depth of the upper and lower panels, respectively. Segunda Angostura is a narrower channel in the Atlantic sector of the Magellan Strait.

Very limited information exists on hydrological characteristics of the Magellan waters. Antezana (1999) reported basic hydrographic features (temperature and salinity) in the main passages of the Strait and suggested that adjacent oceanic waters were warmest in the Atlantic and saltiest in the Pacific sectors, maintaining an along-strait horizontal T-S gradient. Precipitations and continental freshwater discharge to the Strait induce patterns of the diluted

98 near surface waters transported to the Atlantic Patagonian shelf (Brun et al., 2020). The large-
99 scale hydrological features as well as seasonal variations of mesoscale circulation may influence
100 turbulence in the Strait, but strong tides and local winds are the most likely generators of
101 turbulence in the shallow Atlantic sector of the MS.

102 To shed light on characteristics of small-scale turbulence in MS, a short field campaign
103 was carried out in the northeastern part of the Strait using a vertical microstructure profiler
104 VMP-500 and acoustic Doppler current profilers (section 2). Patterns of tidal currents during the
105 microstructure measurements are described in section 3.1. Sections 3.2 and 3.3 present several
106 examples of the TKE dissipation rate profiles comparing the level of turbulence in well-mixed
107 water interior of MS (section 3.3) with turbulence intensity (illustrated by log-normal
108 distribution functions of the dissipation rate) of homogeneous non-stratified layers in other
109 kindred oceanic regions. Specifics of turbulence and mean current shear profiles in the BBL of
110 Segunda Angostura are discussed in section 3.4 vis-à-vis our own measurements carried out in
111 various tidally affected shallow seas. The main results are summarized in section 4, including a
112 comparison of turbulence measurements in narrow tidal channels elsewhere.

113 **2 Measurements**

114 Turbulence and stratification in the Strait were measured using a Vertical Microstructure
115 Profiler, VMP-500, (http://rocklandscientific.com/products/profilers/vmp-500/). Airfoil probes
116 were used to estimate small-scale shear, enabling the calculation of TKE dissipation rate $\varepsilon(z)$, z
117 being the (downward) vertical coordinate. An accelerometer, pressure sensor and a SeaBird
118 temperature-conductivity package provided precise salinity, temperature and potential density
119 profiles. The airfoil sensors were calibrated by Rockland Scientific prior to and after the field
120 campaign. The measurements were taken from a medium-size fishing boat, Marypaz II. The ship
121 was equipped with A-frame at the rear deck, which was used to recover the VMP after each cast
122 conducted in a free-falling mode with a thin tethered cable of neutral buoyancy. We were able to
123 keep the VMP sinking velocity constant, $W \sim 0.7$ ms^{-1} (see Appendix), with a sharp drop off to
124 zero at the end of the casts (usually at ~ 1-2 m above the bottom)

125 A shipboard acoustic Doppler current profiler (ADCP) measured vertical profiles of
126 zonal $u(z)$ or $u(\zeta)$ and meridional $v(z)$ or $v(\zeta)$ velocity components. Here, the distance

from the sea surface z, $\zeta = z_B - z$ is a distance from the sea floor in meters above the bottom (mab) and z_B is the bottom depth in point at the time of measurements. A Teledyne Workhorse sentinel ADCP operated at 600 kHz with high vertical resolution (1-m bin size), but the measurements were restricted to the depth range z = 1 - 49 m. Processing of the VMP and ADCP data followed well-established methodology adopted during our previous field campaigns (e.g., Lozovatsky et al., 2019, 2021; see also Roget et al., 2006 and Goodman et al., 2006). Multiple GPS systems were on board, but an automatic weather station was not present; thus, the meteorological conditions at Punta Arenas during the cruise were used as local.

The VMP-500 was successfully deployed at eight stations near the eastern and western ends of Segunda Angostura (SA) of the Magellan Strait (Figure 1). The first test station was taken on March 2 near the coast (the bottom depth z_b ~ 21 m) under calm weather conditions (wind speed 2-3 ms^{-1}). This appears to be the only VMP station wherein a weak but distinguishable temperature, salinity and density stratifications of the water column were observed. On March 3, a bottom-mounted ADCP mooring was setup in the northern part of SA (see Figure 1), but the VMP measurements on March 3 and 4 were suspended due to rough seas (wave height up to 2 m) and high winds that periodically exceeded 10-12 ms^{-1}. Toward the end of the day of March 5 the stormy wind ceased, permitting to conduct four VMP stations in the central part of SA (closer to its eastern entrance, φ = 52^o 39’58” - 52^o 42’7” S, λ = 70^{o}19’0” - 70^{o}15’51” W; with z_b varying from 30 to 57 m). The measurements continued on March 6 at three stations across the Strait about four miles to the west off the western SA entrance (φ = 52^{o}53’54” - 52^{o}49’5” S, λ = 70 ^{o}49’59” - 70 ^{o}38’58” W with z_b varying from 26 to 57 m). Positions of all VMP stations are shown in Figure 1.

3 Results

3.1 Tidal flow

Basic tidal characteristics in the SA area of MS are given in Figure 2 for two main days of VMP measurements (March 5-6, 2019). The ADCP current components $u(\varsigma,t)$ and $v(\varsigma,t)$ at the mooring location are shown in Figure 2a and the tidal elevation $\eta_{td}(t)$ and tidal ellipses are in Figure 2b. It appears that a semidiurnal tide ($\omega_{td} = 1.41\times10^{-4}$ s^{-1}) with current amplitude ~ 2

ms^{-1} and surface elevation ~ 1.5 m was a dominant background force governing mean currents that generated small-scale turbulence in the SA region. The tidal ellipses (Figure 2b) are highly stretched in NE-SW direction along the SA axis in the middle of the narrow channel.

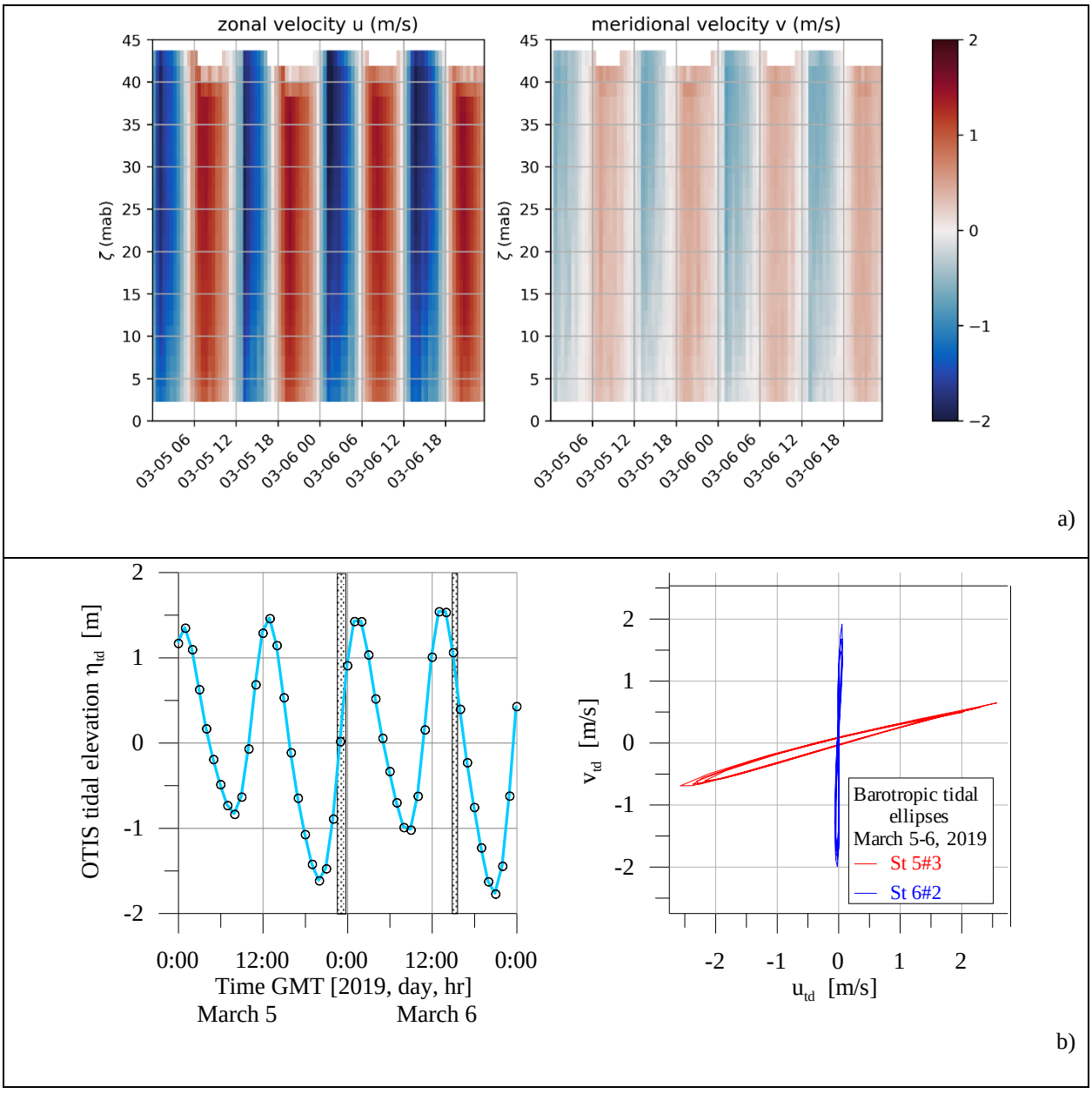

Figure 2. a) - ADCP current components at the mooring location (see Figure 1) for March 5-6, 2019 (color scale in ms^{-1}; b) left - tidal elevation in SA based on modeling data of OTIS (OSU Tidal Inversion Software, courtesy of S. Erofeeva; https://www.tpxo.net/otis). Periods of VMP measurements are marked by grey segments; b) right – OTIS barotropic tidal ellipses in SA for St.5#3 and St. 6#2.

To the west of SA, the dominant tidal current was in the S-N direction with a large amplitude meridional component ($v_{td} \approx \pm 2$ ms^{-1}) and a very small zonal component ($u_{td} \approx \pm 0.07$

164 ms^{-1}). Note that the VMP measurements were taken during rising tide on March 5 and during
165 subsiding tide on March 6, both not at the periods of maximum tidal velocities due to the
166 operational constrains.

167 ### 3.2 MS turbulence: stable ambient stratification

168 Figure 3 shows the TKE dissipation rate profile $\varepsilon(\zeta)$ obtained on March 2 at the
169 beginning of field campaign under light winds (2-3 ms^{-1}).

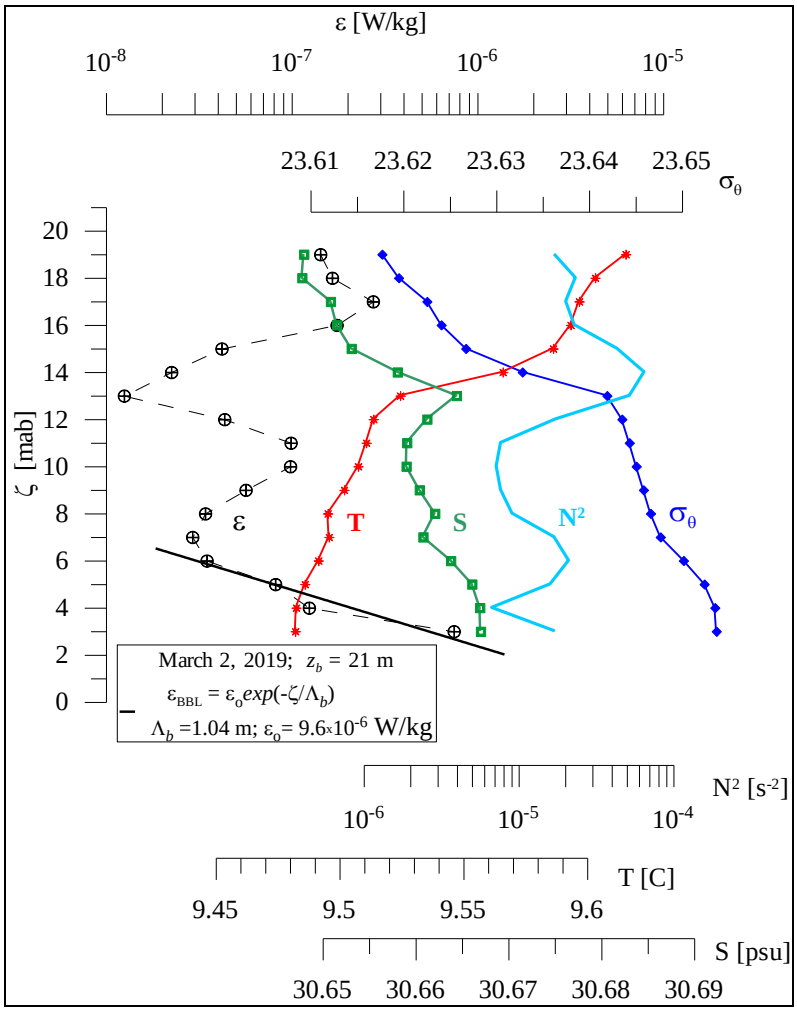

170

171 **Figure 3**. Profiles of the TKE dissipation rate $\varepsilon(\zeta)$, temperature $T(\zeta)$, salinity $S(\zeta)$, potential
172 density $\sigma_\theta(\zeta)$, and squared buoyancy frequency $N^2(\zeta)$ observed under light winds to the west from
173 SA. Here ζ is the distance above the bottom in meters (mab).

174 The background density stratification was characterized by $N^2 \sim 2\times10^{-5}$ s^{-2} for the upper
175 weakly stratified 5 meters of the water column ($\zeta >$ 16 mab), increasing to $\sim 6\times10^{-5}$ s^{-2} in a

narrow, $\zeta =$ 13 - 16 mab, pycnocline (thermocline). Then it generally decreased to $N^2 \sim (0.9-2)\times 10^{-5}$ s^{-2} below the pycnocline ($\zeta <$ 11 - 12 mab). The TKE dissipation rate profile shows relatively high $\varepsilon \approx (1-2)\times 10^{-7}$ Wkg^{-1} in the near surface layer, decreasing to $\varepsilon \sim 10^{-8}$ Wkg^{-1} in the pycnocline. Starting from ζ ~ 6 mab, however, $\varepsilon(\zeta)$ clearly exhibited an exponential growth toward the seafloor (black line in Figure 3), reaching $\varepsilon \sim 8\times 10^{-7}$ Wkg^{-1} at ζ ~ 3 mab. Note that at this shallow station the VMP did not descend closer to the bottom, where ε could perhaps rise by another order of magnitude. The TKE dissipation in the interior of stratified water column, $\varepsilon \sim (1-3)\times 10^{-8}$ Wkg^{-1}, appears to be comparable with (but at the higher end of) the dissipation estimates obtained in our previous measurements on shallow stratified *tidal* shelves elsewhere (see $\varepsilon(\zeta)$ profiles presented later in Figure 6). Note that even in narrow tidal channels (e.g., Sansum Narrows, which separates Vancouver and Saltspring Islands in British Columbia, Canada; flooding tide of ~ 2 ms^{-1}) turbulence is strongly affected by layers of stable stratification, dropping $\varepsilon < 10^{-8}$ Wkg^{-1} (Wolk & Lueck, 2012).

3.3 MS turbulence: well-mixed water interior

After stormy winds (10-12 ms^{-1}) on March 4, the water column in SA was almost completely mixed, being characterized by very low buoyancy frequency N^2 in the range $2\times(10^{-7}-10^{-6})$ s^{-2}. Figure 4 shows vertical profiles of $N^2(\zeta)$, $Sh^2(\zeta)$ (the squared vertical shear, ship-based ADCP measurements), the gradient Richardson number $Ri(\zeta) = N^2(\zeta)/Sh^2(\zeta)$ and $\varepsilon(\zeta)$ to demonstrate properties of well-mixed tidal flow in the MS. Vertical structure of all variables in Figure 4 consists of two distinct layers. The first is the bottom boundary layer, where the dissipation rate exponentially increases with depth ($\zeta < \zeta_{BBL} \approx 8$ mab) mirroring an exponential increase of vertical shear and corresponding decrease of $Ri(\zeta)$. Although $N^2(\zeta)$ shows slight increase in two meters just above the seafloor, the values of $N^2 < 7\times 10^{-7}$ s^{-2} are still extremely low.

Another major layer covers the water column above the BBL ($\zeta > \zeta_{BBL}$), where the shear and the dissipation rate vary around the means $\langle\varepsilon\rangle = 6.8\times 10^{-7}$ Wkg^{-1} and $\langle Sh^2\rangle = 1.1\times 10^{-4}$ s^{-2}

for an example in Figure 4. Statistical behavior of such random variable as ε can be specified in terms of the cumulative probability distribution function $CDF(\varepsilon)$, which is shown in Figure 5 by red pentagrams, calculated using all dissipation samples pertained to the depth range between z_o = 5 m and z_{BBL} = 25 - 50 m depending on the BBL height ζ_{BBL} in every specific VMP cast.

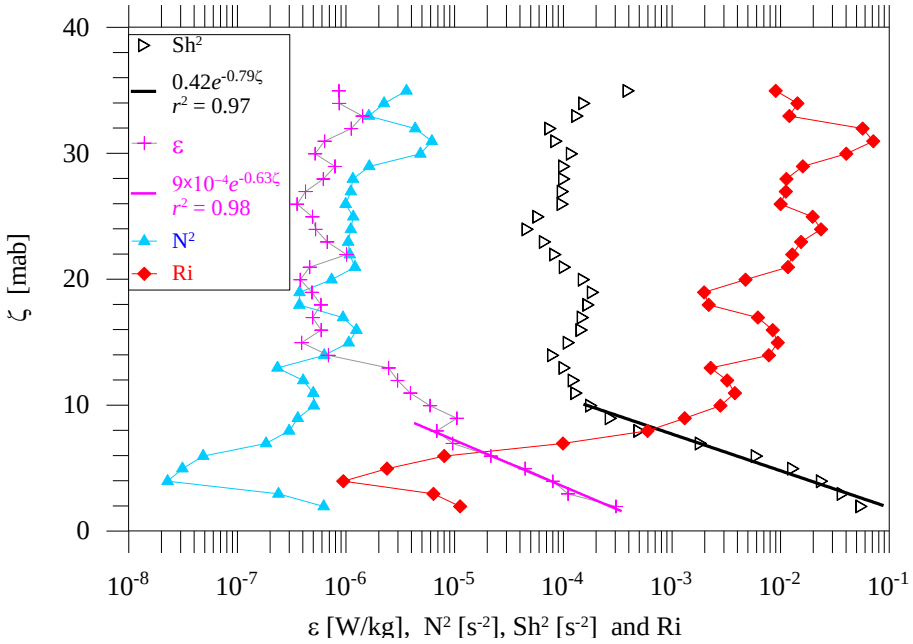

Figure 4. An example of the vertical profiles of squared buoyancy frequency $N^2(\zeta)$, mean shear $Sh^2(\zeta)$, gradient Richardson number $Ri(\zeta)$, and dissipation rate $\varepsilon(\zeta)$ obtained on March 6 in the mixed waters of MS (signified by very small values of $N^2(\zeta)$ in the entire water column). Station 6#2 in Figure 1.

To compare turbulence intensity in homogeneous waters of MS with non-stratified turbulence in oceanic regions elsewhere, Figure 5 shows several examples of $CDF(\varepsilon)$ obtained for surface mixed layers (SML) in the northern (Jinadasa et al., 2016) and southwestern (Lozovatsky et al., 2019) Bay of Bengal (BoB-13 and BoB-18, respectively) and in the Gulf Stream region (GS-15). Those $CDF(\varepsilon)$ were calculated for z = 10 to 30 m for relatively shallow SML underlain by a sharp pycnocline in both BoB regions (moderate local winds) and z = 10 to 50 m in a deep, well-developed SML for GS-15 (Lozovatsky et al., 2017a).

As expected, all $CDFs(\varepsilon)$ in Figure 5 are well approximated by lognormal probability distribution of the Gurvich & Yaglom (1967) model as well as numerous data obtained in non-stratified marine layers (e.g., Lozovatsky et al., 2017b; McMillan & Hay, 2017). Furthermore, Figure 5 indicates that turbulence in SA is much stronger than that typically observed in oceanic SML under similar (low and moderate) winds. The median value of the TKE dissipation rate in the MS above the BBL $\varepsilon_{med}^{MS} = 1.2\times10^{-6}$ Wkg^{-1} is an order of magnitude higher than that in the SML *CDFs* shown in Figure 5, where $\varepsilon_{med}^{SML} \approx (2-7)\times10^{-7}$ Wkg^{-1}. Such high level of turbulence appears to be governed by shear instability developed across the entire water column in the SA region, where $\langle Sh^2 \rangle = 1.1\times10^{-4}$ s^{-2} and highly subcritical *Ri* values, varying above the BBL mostly in the range *Ri* ~ 0.01 – 0.1.

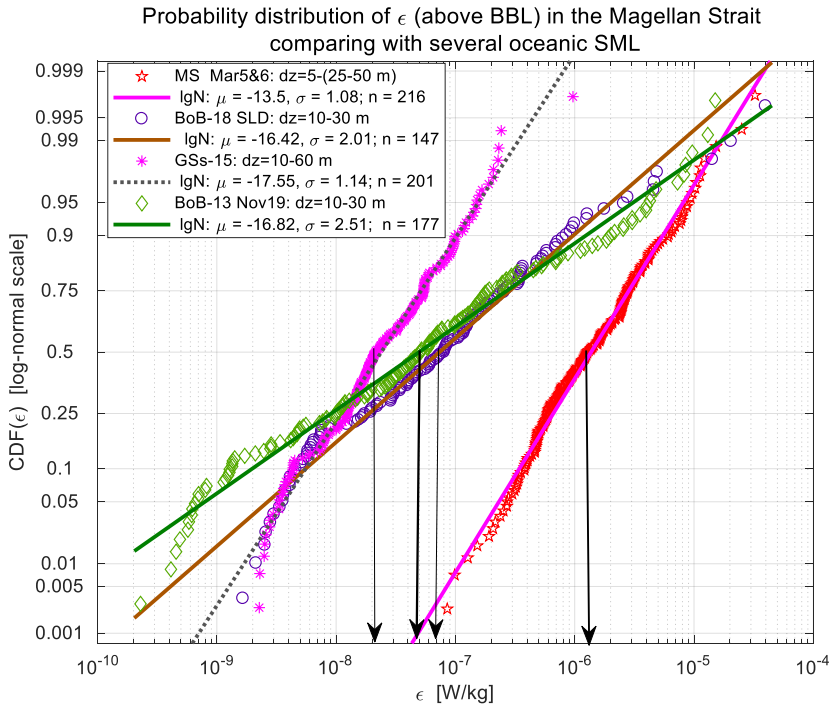

Figure 5. Cumulative distribution functions of the dissipation rate $CDF(\varepsilon)$ for mixed water interior of the Magellan Strait (MS 2019, March 5&6 data) and examples of $CDF(\varepsilon)$ for oceanic surface mixed layer (SML) under light and moderate winds. Those measurements were taken in the northern and southern Bay of Bengal (BoB-13 and BoB-18, respectively) and in the Gulf Stream (GS-15). The depth ranges selected for $CDF(\varepsilon)$ calculation, the number of CDF samples *n* and parameters of lognormal approximations of the empirical distributions μ and σ are in the legend. The arrows point to the corresponding median values.

3.4 MS turbulence: BBL

The BBL in well-mixed waters of MS was not distinct in thermohaline profiles due to very small differences in temperature, salinity, and density near the bottom, but the BBL was easy to define in the profiles of the squared mean shear $Sh^2(\zeta)$ and the dissipation rate $\varepsilon(\zeta)$. The TKE dissipation profiles $\varepsilon(\zeta)$ shown in Figures 3 and 4 clearly indicate that starting from some distance above the bottom $\zeta_{BBL} = z_b - z_{BBL}$, the dissipation rate sharply (exponentially) increases toward the seafloor. All $\varepsilon(\zeta)$ profiles in the MS showed an exponential dependence ε on ζ

$$\varepsilon(\zeta) = \varepsilon_b e^{-\zeta/\Lambda} \quad (1)$$

where ε_b is the dissipation rate near the bottom and Λ a characteristic external length scale for shear generated turbulence by mean (tidal) flow. Two additional $\varepsilon(\zeta)$ profiles typical of March 5 and 6 are given in Figure 6 along with several profiles of $\varepsilon(\zeta)$ obtained elsewhere in shallow tidal seas, where an exponential decrease of ε with ζ in BBL is demonstrated. These latter data were collected in the Changjiang River Diluted Waters (YS-CDW) in the southwestern Yellow Sea (Lozovatsky et al., 2012), in the IEODO region (YS-IEODO) in the southeastern Yellow Sea (Lozovatsky et al., 2015) as well as on the North Carolina (NC) shelf (Lozovatsky et al., 2017a). Note that an exponential decay of $\varepsilon(\zeta)$ has been suggested by St. Laurent et al. (2002) for deep-ocean BBL as a possible model of $\varepsilon(\zeta)$ for turbulence generated by internal tidal energy flux propagated upward over rough abyssal bathymetry.

All dissipation rate profiles in shallow BBL shown in Figure 6 can be well-approximated by formulae (1) with coefficient of determination r^2 = 0.94 - 0.99. The tallest turbulent BBL with exponentially varying $\varepsilon(\zeta)$ was observed in the YS-IEODO region (ζ_{BBL} ~ 15 mab, $\Lambda = 3.1$ m) while a characteristic height of such BBL in other regions was ζ_{BBL} ~ 8 - 9 mab with $\Lambda = 1.4 - 1.6$ m. It is worth noting that for all $\varepsilon(\zeta)$ profiles in Figure 6, the external turbulent scale $\Lambda \sim 0.2\zeta_{BBL}$, which is a typical value for boundary-induced turbulence (e.g., Monin &

Yaglom 1971). An exponential decrease of $\varepsilon(\zeta)$ within the YS-IEODO BBL has been observed by Lozovatsky et al. (2015) who argued that weak remnant stable stratification therein could cause a faster decrease of ε with ζ compared to an inverse-distance decay of $\varepsilon(\zeta)$ that has been discussed in numerous publications (e.g., Sanford & Lien 1999; Lozovatsky et al., 2008; McMillan et al, 2016) in relation to marine BBL.

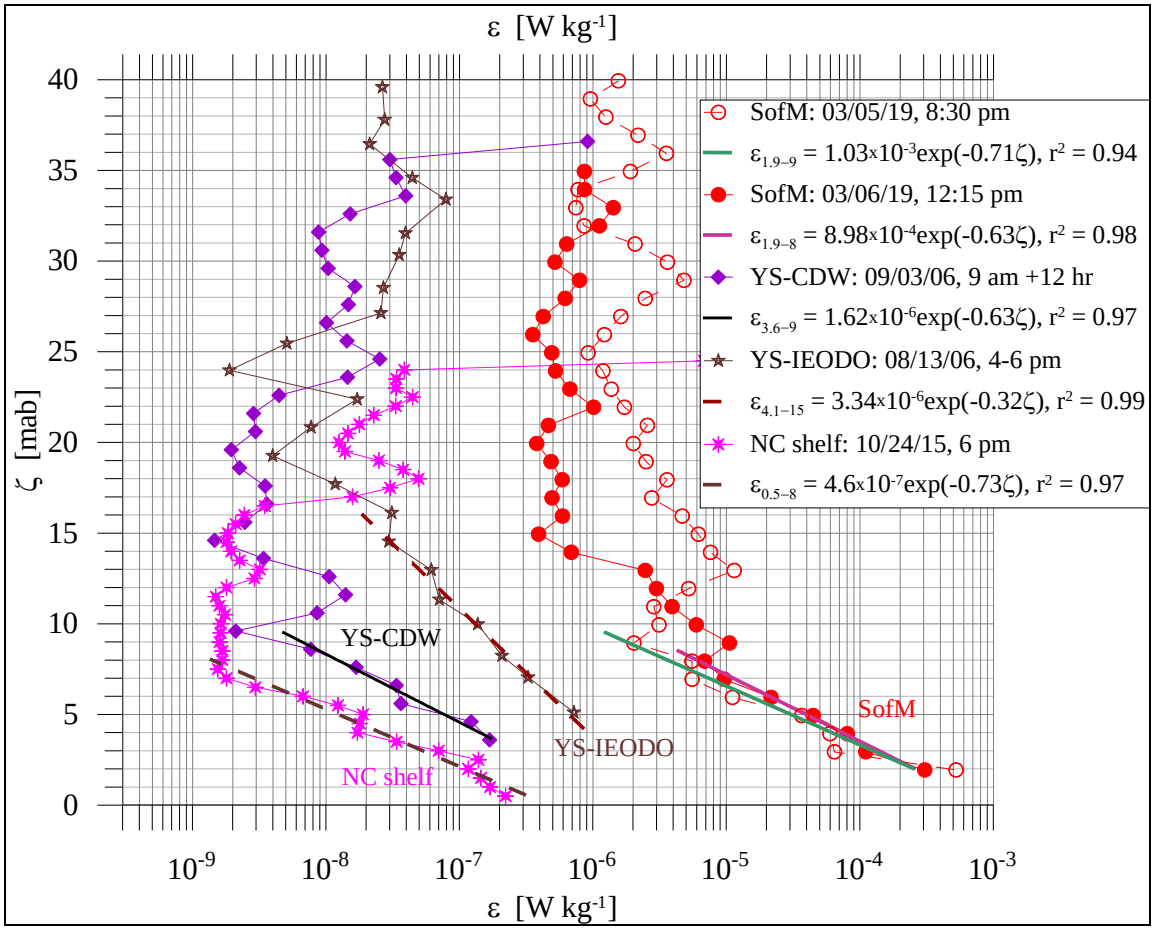

Figure 6. Examples of $\varepsilon(\zeta)$ profiles showing an exponential increase of ε in the BBL toward the seafloor at two stations in the Strait (March 5#3 and March 6#2, 2019) and typical $\varepsilon(\zeta)$ profiles measured in shallow tidal seas that exhibit exponential dependences $\varepsilon(\zeta) \sim \varepsilon_b exp(-\zeta/\Lambda)$ in BBL. Here, ε_b is a dissipation rate near the bottom and Λ a characteristic length-scale of BBL turbulence. Those data have been reported by Lozovatsky et al. (2017a) for North Carolina shelf (NC shelf) and by Lozovatsky et al (2012, 2015) for Changjiang River Diluted Waters (YS-CDW) in the southwestern sector of Yellow Sea, and for the IEODO region (YS-IEODO) in the southeastern YS, respectively. Parameters pertinent to the exponential approximations $\varepsilon(\zeta)$ (straight lines) are in the legend.

While such an assumption for the MS BBL with very small $N^2 \approx 10^{-7}–10^{-6}$ s^{-2} should be considered with circumspection, Sakamoto & Akitomo (2006) argued that even weakly stable stratification on the order of $N^2 \approx 10^{-6}$ s^{-2} may suppress BBL mixing specifically at high latitudes. Rotation of tidal flow may also have a stabilizing effect on BBL turbulence, similar to stable stratification and/or the Coriolis forces (e.g., Sakamoto & Akitomo 2008; Yoshikawa et al. 2010). Tidal ellipses in the SA region are so narrow (Figure 2b), however, that the flow resembles a reversing rather than a rotating tide.

Thus, the exponential behavior of $\varepsilon(\zeta)$ in the MS BBL as well as in several tidal shallow seas could be considered to have different dynamics than log-layer boundary turbulence. The clue is the exponential increase of mean squared shear in the BBL, which was presented as an example for one of the stations in Figure 4. To verify the dependence between shear and dissipation rate, we plotted ε vs. Sh^2 for MS stations with z_b < 49 m, where both VMP and ADCP returned data close to the seafloor (1.3 – 2.9 mab). The data from "exponential BBLs" are shown in Figure 7 by large symbols with adjacent numbers indicating the height from the seafloor. If turbulence is solely generated by mean shear, for stationary turbulence the production $K_M Sh^2$ term is balanced by viscous dissipation ε as

$$K_M Sh^2 = \varepsilon, \tag{2}$$

where K_M is the eddy viscosity that parametrizes the vertical momentum flux $\overline{u'w'} = -K_M Sh$. In Figure 7, the success of Eq.2 as an approximate empirical regression between ε and Sh^2 in the BBLs is apparent with high coefficients of determination r^2 = 0.92 - 0.98. The result signifies that in the MS BBL (at $\zeta > \sim 2$ mab), the eddy viscosity K_M is independent of ζ (constant with height), varying in a relatively narrow range $K_M = (0.83 - 3.4) \times 10^{-3}$ m^2 s^{-1}, though it depends on the location in the Strait and the time of measurement (i.e., tidal phase); also see Ross et al. (2019) who reported substantial tidal variability of K_M in a coastal plain estuary in the French Atlantic Coast. Note that on March 5 and March 6, the VMP measurements were taken in approximately the same transitional phase between low and high tide indicated in Figure 2.

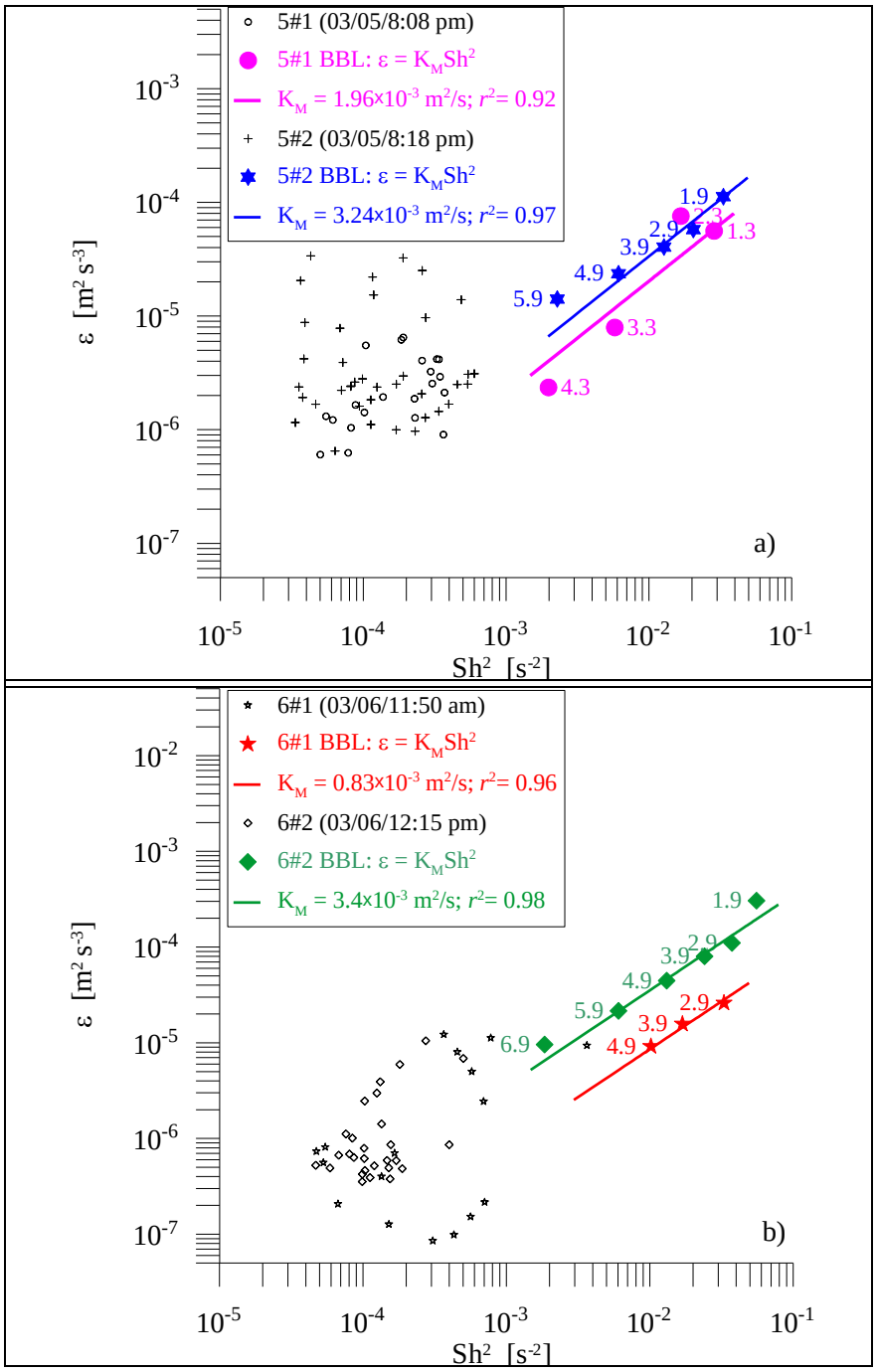

303

304 **Figure 7.** The TKE dissipation rate ε vs. the squared vertical shear Sh^2: a) - stations 5#1 and 5#2, b) -
305 stations 6#1 and 6#2. Colored symbols belong to BBLs (see examples in Figures 4 and 6); the numbers
306 adjacent to the symbols specify the height above the bottom in mab. Parameters pertinent to the
307 approximations by Eq. 2 (eddy viscosity and r^2) are in the legend.

308

The estimates of K_M allow assessing the possible thickness of the turbulent BBL h_{tbl} over a bottom roughness. Yoshikawa et al. (2010) suggested that rotating tidal currents over a large continental shelf affect the thickness of the Ekman BBL. Considering, however, that background rotation associated with strong reversing tidal currents is negligible in such narrow channels as SA, it is not possible to use the classical Ekman BBL height formulae in this case (Pedlosky 1987), but analogous to the Stokes oscillatory boundary layer (e.g., Krstic & Fernando, 2001), thickness of the reversing tidal turbulent BBL h_{tbl} over rough bathymetry composed of hard substratum (Simeoni et al., 1997) can be written as

$$h_{tbl} = \left(\frac{2K_M}{\omega_{td}} \right)^{1/2}, \quad (3)$$

where $\omega_{td} = 1.41 \times 10^{-4}$ s^{-1} the semidiurnal tidal frequency. Using the estimates for the present case $K_M = (0.83 - 3.4) \times 10^{-3}$ m^{2}s^{-1}, h_{tbl} is found to be in the range 3.5 – 6.9 m. This is in general agreement with data shown in Figure 7, where the height of the "exponential BBL" varies between 4.3 and 6.9 mab. Thus, reversing tidal currents in a channel of the ilk of SA may create a specific regime of strong ($\varepsilon_b \sim 10^{-3}$ Wkg^{-1}) bottom-generated turbulence, which can be characterized by a constant eddy viscosity and a TKE dissipation rate that exponentially decays toward the water interior. The upper boundary of the exponential decay region of turbulence in the northern MS is 4 - 7 mab for a transitional tidal phase, characterized by a characteristic tidal velocity ~ 1 ms^{-1} and eddy viscosity ~10^{-3} m^{2}s^{-1}.

4 Summary

First ever measurements of turbulence in the northeastern Strait of Magellan were taken during March 2 – 6, 2019. A vertical microstructure profiler (VMP) and a shipboard acoustic Doppler current profiler (ADCP) were used to obtain estimates of the TKE dissipation rate and vertical shear at several stations (the bottom depth ranged between 25 and 55 m), respectively, in the Segunda Angostura region to the north of Punta Arenas. During the field campaign, tidal elevation varied in the range $\pm \sim 1.5$ m. At the time of microstructure measurements, the speed of reversing tidal currents was 0.8 - 1.2 ms^{-1}. After a mild storm, entire water column became well mixed with the median TKE dissipation rate above the bottom boundary layer $\varepsilon_{med}^{MS} = 1.2 \times 10^{-6}$ Wkg^{-1}, which was about an order of magnitude higher compared to the surface

mixed layer turbulence measured under moderate winds in typical ocean. This was associated with strong, $(1-2)\times10^{-2}$ s^{-1}, vertical shear in the water interior that yielded gradient Richardson numbers $Ri < 10^{-1} - 10^{-2}$, which is well below the lower critical value threshold favorable for shear-induced turbulence. The dissipation rate near the seabed in MS was close to $\varepsilon_b \approx 10^{-3}$ Wkg^{-1}. Note that Thomson et al. (2012) reported the tidally-induced near-bottom dissipation rate in the Puget Sound, WA, USA, which was as high as that measured in the Strait of Magellan, namely $\varepsilon_b \sim 10^{-4} - 10^{-3}$ Wkg^{-1}. During microstructure measurements, the tidal-current generated turbulent BBL height was ~ 4 - 7 m, with an exponential decay of the dissipation rate and the vertical shear toward the water interior. In the exponentially varying regime, the eddy viscosity was found to be $K_M = (0.83-3.4)\times10^{-3}$ m^2s^{-1}, independent of the vertical coordinate ζ but dependent on tidal phase and location. Note that the eddy viscosity as high as $10^{-2} - 10^{-1}$ m^2s^{-1} has been reported by Ross et al. (2019) for the spring tide in a plain estuary on the French Atlantic Coast. The results of the pilot field campaign described in this paper provided first yet limited information on the specifics of turbulence in the Magellan Strait, calling for further comprehensive investigations.

Acknowledgements

We are greatly thankful to the crew of the vessel Marypaz II for immense help during the VMP measurements. The research cruise was funded by the Marine Energy Research & Innovation Center of Chile (MERIC), CORFO project 14CEI2-28228. Chilean scientists were supported by MERIC and Research Internationalization Grant of the Pontificia Universidad Católica de Chile (grant no. PUC1566). The University of Notre Dame participants were partially supported through the 2018-2019 Luksic Family Collaboration Grant Award (https://international.nd.edu/faculty-research/grants-and-funding/luksic-family-collaboration-grant/luksic-family-collaboration-grant-awardees/). During the preparation of this paper, Notre Dame group was supported by ONR Grants N00014-17-1-3195 (dealing with air-sea interactions with EM ducting) as well as N00014-18-1-2472 (shelf/BBL turbulence with applications to marine fog genesis).

Conflict of Interest

The authors declare no conflicts of interest relevant to this study.

Data Availability Statement

The data used in this paper is available upon request from the corresponding author. Data management repository available at https://drive.google.com/drive/folders/1mVA--r4dQ9qVBgSmxNQILcQJ_5ypC_93?usp=sharing

References

Acevedo, J., Plana, J., Aguayo-Lobo, A., & Pastene, L. A. (2011). Surface feeding behavior of humpback whales in the Magellan Strait. *Revista de Biologia Marina y Oceanografia 46*(*3*), 483-490. http://dx.doi.org/10.4067/S0718-19572011000300018

Brun, A.A., Ramirez, N., Pizarro, O., & Piola, A.R. (2020). The role of the Magellan Strait on the southwest South Atlantic shelf. *Estuarine, Coastal and Shelf Science 237* (2020) 106661, 1-11. https://doi.org/10.1016/j.ecss.2020.106661

Garreaud, R., Lopez, P., Minvielle, M., & Rojas, M. (2013). Large-scale control on the Patagonian climate. *Journal of Climate*, *26*(1), 215-230.

Goodman, L., Levine, E.R., & Lueck, R.G. (2006). On measuring the terms of the turbulent kinetic energy budget from an AUV. *Journal of Atmospheric and Oceanic Technology*, *23*, 977–990. http://journals.ametsoc.org/doi/abs/10.1175/JTECH1889.1

Guerra, M., & Thomson, J. (2017). Turbulence measurements from five-beam acoustic doppler current profilers. *Journal of Atmospheric and Oceanic Technology*, *34*, 1267–1284. https://doi.org/10.1175/JTECH-D-16-0148.1

Horwitz, R., & Hay, A. (2017). Turbulence dissipation rates from horizontal velocity profiles at mid-depth in fast tidal flows. *Renewable Energy*, *114*, 283–296, doi:10.1016/j.renene.2017.03.062

Jinadasa, S.U.P., Lozovatsky, I., Planella-Morató, J., Nash, J.D., MacKinnon, J.A., Lucas, A.J., Wijesekera, H.W., & Fernando, H.J.S. (2016). Ocean turbulence and mixing around Sri Lanka and in adjacent waters of the northern Bay of Bengal. *Oceanography 29,* 170–179. http://dx.doi.org/10.5670/oceanog.2016.49

Krstic, A., & Fernando, H.J.S. (2001). The nature of rough-wall oscillatory boundary layers. *J Hydraulic Research, 39*(*6*), 655-666. https://doi.org/10.1080/00221686.2001.9628294

Lozovatsky, I.D., Liu, Z., Hao, W., & Fernando, H.J.S. (2008). Tides and mixing in the northwestern East China Sea. Part II: The near-bottom turbulence. *Continental Shelf Research, 28*(2), 338-350. doi:10.1016/j.csr.2007.08.007

Lozovatsky, I., Liu, Z., Fernando, H.J.S., Armengol, J., & Roget, E. (2012). Shallow water tidal currents in close proximity to the seafloor and boundary-induced turbulence. *Ocean Dynamics, 62*, 177-201. doi:10.1007/s10236-011-0495-3.

Lozovatsky, I., Lee, J.-H., Fernando, H.J.S., Kang, S.K., & Jinadasa, S.U.P. (2015). Turbulence in the East China Sea: The summertime stratification. *Journal Geophysical. Research: Oceans, 120*, 1856–1871. doi: 10.1002/2014JC010596

Lozovatsky, I, Planella-Morato, J., Shearman, K., Wang, Q., & Fernando, H.J.S. (2017a). Eddy diffusivity and elements of mesoscale dynamics over North Carolina shelf and contiguous Gulf Stream waters. *Ocean Dynamics 67*, 783-798. doi 10.1007/s10236-017-1059-y

Lozovatsky, I., Fernando, H.J.S., Planella-Morato, J., Liu, Z., Lee, J.-H., & Jinadasa, S.U.P. (2017b). Probability distribution of turbulent kinetic energy dissipation rate in ocean: Observations and approximations. *Journal Geophysical Research: Oceans 122*, 8293-8308. doi 10.1002/2017JC013076

Lozovatsky I., Pirro, A., Jarosz, E., Wijesekera, H.W., Jinadasa, S.U.P., & Fernando, H.J.S. (2019). Turbulence at the periphery of Sri Lanka dome. *Deep Sea Research* II, *168*, 104614:1-8. https://doi.org/10.1016/j. dsr2.2019.07.002

Lozovatsky, I., C. Wainwright, E. Creegan, and H. J. S. Fernando, 2021: Ocean turbulence and mixing near the shelf break southeast of Nova Scotia. *Boundary-Layer Meteor.* **181**, 425-441. https://doi.org/10.1007/s10546-020-00576-z

Lutz, V., Frouin, R., Negri, R., Silva, R., Pompeu, M., Rudorff, N., Cabral, A., Dogliotti, A., & Martinez, G. (2016). Bio-optical characteristics along the Straits of Magallanes. *Continental Shelf Researc*h *119*, 56–67.

McMillan, J.M., Hay, A.E., Lueck, R.G., & Wolk, F. (2016). Rates of dissipation of turbulent kinetic energy in a high Reynolds number tidal channel. *Journal Physical Oceanography, 33*, 817–837, doi:10.1175/JTECH-D-15-0167.1

McMillan, J.M., & Hay, A.E. (2017). Spectral and structure function estimates of turbulence dissipation rates in a high-flow tidal channel using broadband ADCPs. *Journal of Atmospheric and Oceanic Technology, 34*, 5–20, doi:10.1175/JTECH-D-16-0131.1.

Medeiros, Carmen & Bjorn Kjerfve. (1988). Tidal characteristics of the Strait of Magellan. *Continental Shelf Research, 8*(8), 947-960.

Monin, A.S., & Yaglom, A.M. (1971). Statistical Fluid Mechanics: Mechanics of Turbulence, 1. MIT Press, Cambridge, MA, 782pp.

Pedlosky, J. (1987). *Geophysical Fluid Dynamics.* 2d ed. Springer-Verlag, 710 pp. https://doi.org/10.1007/978-1-4612-4650-3

Ross, L., Huguenard, K., & Sottolichio, A. (2019).: Intratidal and fortnightly variability of vertical mixing in a macrotidal estuary: The Gironde. *Journal of Geophysical Research: Oceans, 124,* 2641–2659. https://doi.org/10.1029/2018JC014456)

Roget, E., Lozovatsky, I., Sanchez, X., & Figueroa, M. (2006). Microstructure measurements in natural waters: Methodology and applications. *Progress in Oceanography 70*, 123-148.

Sakamoto, K., & Akitomo, K. 2006: Instabilities of the tidally induced bottom boundary layer in the rotating frame and their mixing effect. *Dynamics of Atmospheres and Oceans* ***41***, 191–211.

Sanford, T.S., and Lien, R.-C. (1999). Turbulent properties in a homogeneous tidal boundary layer. *Journal of Geophysical Research: Oceans 104*, (C1), 1245–1257.

Simeoni, U., Fontolan, G., & Colizza, E. (1997). Geomorphological characterization of the coastal and marine area between Primera and Segunda Angostura, Strait of Magellan (Chile) *Journal of Coastal Research, 13*, No.3, 916-924.

St. Laurent, L.C., Simmons, H.L., & Jayne, S.R. (2002). Estimating tidally driven mixing in the deep ocean, *Geophysical. Research Letters 29*(23), 2106, doi:10.1029/2002GL015633

Thomson, J., Polagye, B., Durgesh, V., & Richmond, M.C. (2012). Measurements of turbulence at two tidal energy sites in Puget Sound, WA, *IEEE Journal of oceanic engineering*, ***37*****(**3), 363-374

Yoshikawa, Y., Endoh, T., Matsuno, T., Wagawa, T., Tsutsumi, E., Yoshimura, H., & Morii, Y. (2010). Turbulent bottom Ekman boundary layer measured over a continental shelf. *Geophysical. Research Letters 37*, L15605. doi: 10.1029/2010GL044156

Wolk, F. & Lueck, R. (2012). VMP turbulence profiler measurements in a tidal channel. *Rockland Technical Note 024*. 2012-06-30. https://rocklandscientific.com/wp-content/uploads /2021/12/TN_024_VMP_in_Tidal_Channels.pdf

Appendix

Examples of the VMP sinking velocity profiles $W(P)$ shown in Fig. A1 indicate fairly undisturbed almost constant $W(P)$ ~ 0.7 m/s during a major portion of the casts and a sharp drop of $W(P)$ to zero at the end of the casts (*P* is pressure).

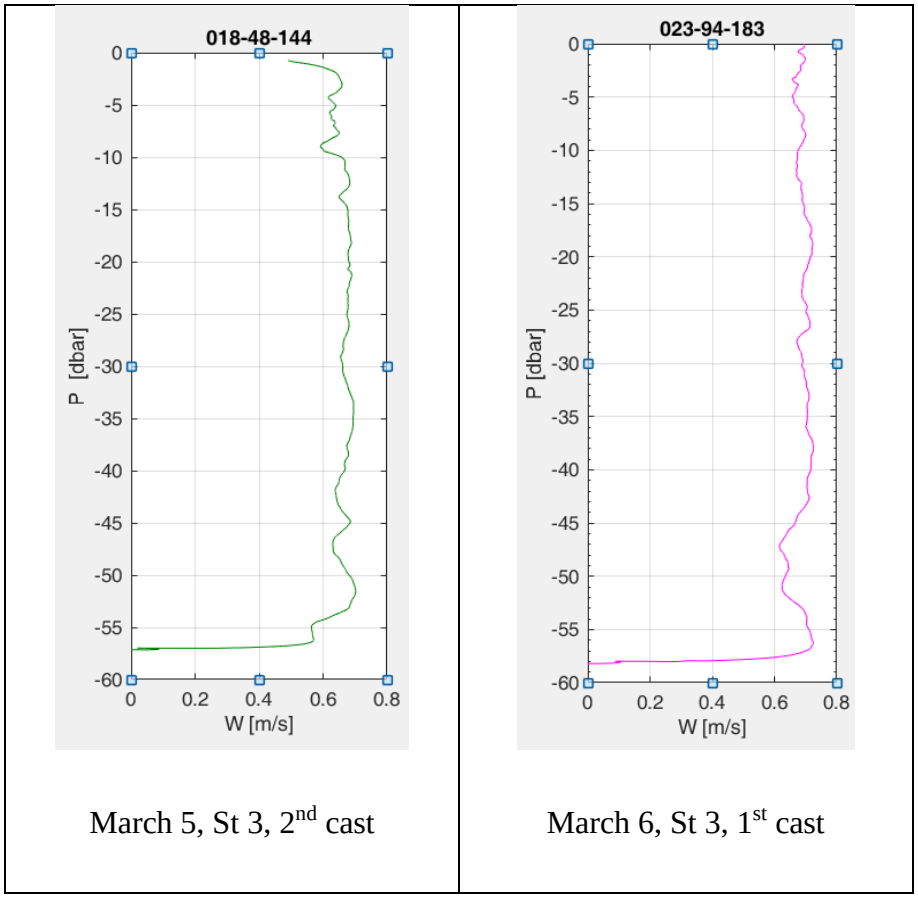

Figure A1. The VMP sinking velocity profiles for two casts taken in the Magellan Strait on March 5 and 6, 2019 (see stations in Figure 1).